IEEE Access
Multidisciplinary | Rapid Review | Open Access Journal

Received April 19, 2019, accepted May 8, 2019, date of publication May 14, 2019, date of current version June 4, 2019.

Digital Object Identifier 10.1109/ACCESS.2019.2916718

Deer Crossing Road Detection With Roadside LiDAR Sensor

JINGRONG CHEN[1], HAO XU[2], JIANQING WU[2], RUI YUE[2], CHANGWEI YUAN[3], AND LU WANG[2]

[1]School of Mathematics and Physics, Lanzhou Jiaotong University, Lanzhou 730070, China
[2]Department of Civil and Environmental Engineering, University of Nevada, Reno, NV 89557, USA
[3]School of Economics and Management, Chang'an University, Xi'an 710064, China

Corresponding authors: Jianqing Wu (jianqingw@nevada.unr.edu) and Changwei Yuan (yuanchangwei@126.com)

This work was supported in part by the Natural Science Foundation of China under Grant 61463026 and Grant 61463027, in part by the Nevada Department of Transportation (NDOT) under Grant P224-14-803/TO #13, in part by the Fundamental Research Funds for the Central Universities under Grant 300102238614, and in part by The Ministry of Education of Humanities and Social Science Project under Grant 18YJAZH120.

ABSTRACT Deer crossing roads are a major concern of highway safety in rural and suburban areas in the United States. This paper provided an innovative approach to detecting deer crossing at highways using 3D light detection and ranging (LiDAR) technology. The developed LiDAR data processing procedure includes background filtering, object clustering, and object classification. An automatic background filtering method based on the point distribution was applied to exclude background but keep the deer (and road users if they exist) in the space. A modified density-based spatial clustering of applications with noise (DBSCAN) algorithm was used for object clustering. Adaptive searching parameters were applied in the vertical and horizontal directions to cluster the points. The cluster groups were further classified into three groups—deer, pedestrians, and vehicles, using three different algorithms: naive Bayes, random forest, and k-nearest neighbor. The testing results showed that the random forest (RF) can provide the highest accuracy for classification among the three algorithms. The results of the field test showed that the developed method can detect the deer with an average distance of 30 m far away from the LiDAR. The time delay is about 0.2 s in this test. The deer crossing information can warn drivers about the risks of deer-vehicle crashes in real time.

INDEX TERMS Deer crossing, object classification, roadside LiDAR, vehicle trajectories.

I. INTRODUCTION

More than 1.5 million traffic crashes involving deer, resulting in about $1.1 billion in vehicle damage and 150 fatalities, are estimated to occur annually from 1998 to 2002 in the United States [1]. The actual number is higher than the reported crashes, as only part of such crashes are reported to authorities [2]. Many solutions have been developed to minimize deer-vehicle collisions, primarily fencing and crossing structures that allow deer to safely cross under or over a road while preventing animals from accessing the road [3], [4]. However, the cost of building crossing structures is usually very expensive. Deer crossing signs are often installed near the road to warn drivers in the areas with high frequency of deer crossing the road. A previous study [5] showed that these signs were not effective to reduce deer-vehicle crash (DVC). On average, motorists responded to the signs by reducing vehicle speeds, but the reduction in speed was too small to be of practical importance [5]. On the other hand, once a sign has been installed, it is rarely removed, even if the wildlife crossing problem no longer exists [6], which provides the incorrect warning to drivers. Compared to those static deer crossing signs, the signs triggered by the real-time deer crossing detection can warn drivers more effectively and accurately [7]. The basic idea of the real-time deer crossing system is that once the sensors detect any deer near the road (before crossing activities), the lights on the sign will be triggered to flash to provide the real-time warning to the nearby drivers. After deer cross the road, the lights will be turned off automatically. The major challenge in the development of the real-time deer crossing system is how to detect the deer crossing in advance with high accuracy.

Several technologies (e.g., cameras or radar) have been used for wildlife crossing detection. There have been studies [8], [9] using high-frequency radio-tracking (VHF) and GPS-based-tracking technologies to track the location of deer. For VHF or GPS based technologies, detection is limited to animals equipped with devices as they do not track the

The associate editor coordinating the review of this manuscript and approving it for publication was Lorenzo Ciani.

non-controlled animals. On the other hand, it is not practical to deploy the detecting devices on all animals. Previous studies [3]–[10] have applied cameras for wildlife crossing detection. The limitation of traditional cameras is that they could not work well during night time or with burning sun (influenced by the lights) [11]. Thermal cameras (infrared cameras) were developed to overcome this limitation [12]. The thermal cameras use infrared radiation to form an image. Thermal cameras can work even in total no-light conditions. With the advanced thermal imaging and digital imaging processing technologies, the speed and position of animals can be calculated from the images captured by thermal cameras [13]. Christiansen *et al.* [14] claimed that their thermal camera-based method can identify wildlife from non-wildlife objects with an accuracy of 93.5% in the range of 3-5m and 77.7% in the range of 10-20m. Out of 20m (65.6ft), the wildlife could not be successfully detected. However, those abovementioned studies indicated that thermal cameras can only detect animals in a limited field of view due to the limited lateral detection range [15]. Radar sensors can also be used for real-time deer crossing detection. Viani *et al.* [16] developed a wildlife road-crossing early-alert system based on multiple Doppler radar sensors. The results of the experiment showed that the system can detect moving objects within 16 meters from the radar with the low time delay (about 1 second). Similar to thermal cameras, radar also has a limited field of view. Which means it could not detect all objects in a 360° lateral view [17]. However, it is difficult to estimate the direction that the deer come from. Therefore, it is not guaranteed that the deer will show up within the field of view. To overcome this issue, several radar sensors need to work together to extend the lateral detection range, which will increase the total cost at the same time [18].

The 360-degree Light Detection and Ranging (LiDAR) technology has the capability to scan the 360° three-dimensional surrounding objects with high accuracy, which can provide an opportunity for real-time deer detection [19]. The LiDAR sensors can work day and night continuously without influence from different light conditions [20]. Furthermore, the LiDAR sensors can work with GPS together to match all scanned points to the right location. LiDAR sensors have been employed for advanced autonomous vehicles for several years to detect road boundary, obstructions and other road users automatically [20]. A series of algorithms [21]–[23] have been developed for object detection using on-board LiDAR. The high price of LiDAR sensor limited the application of LiDAR sensors for many years, but the price of LiDAR sensors has dropped to the several thousand dollars level, making it possible for new LiDAR applications. Recently, roadside LiDAR-enhanced infrastructure developed by the authors has been a new application of LiDAR serving connected-vehicles. Inspired by the previous work and the advantage of the LiDAR [24]–[27], the authors started to use roadside LiDAR for deer crossing detection. This paper provides an innovative approach to detecting deer crossing in real-time with a LiDAR sensor. The detailed data processing algorithms were provided. The field study showed that the developed procedure can detect the deer in advance with high accuracy. The limitations of this research and discussions about further studies were also summarized in this paper.

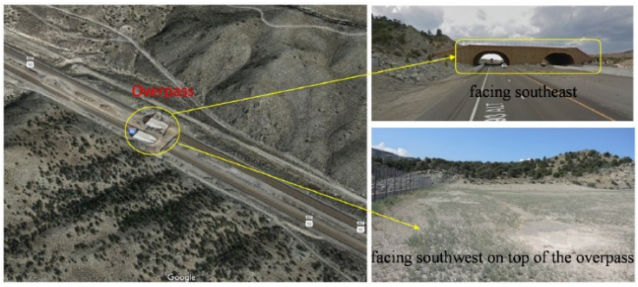

FIGURE 1. Wildlife overpass-data collection site.

II. ROADSIDE LiDAR AND DATA COLLECTION SITE

The cost-effective VLP-16 sensor was selected in this research with consideration of its performance and price. The current cost is $3,900 per unit based on the quote provided by Velodyne-the manufacture of VLP-16. The VLP-16 LiDAR is applied for wildlife data collection in this research. The VLP-16 LiDAR can create 360 3D point cloud by using 16 laser/detector pairs mounted in a compact housing. The housing rapidly spins to scan the surrounding environment with a range of 100 m (328 ft). The LiDAR has the rotational speed of 5-20 rotations per second, which can generate 600,000 3D points per second. It can cover 360° horizontal field of view and a 30° vertical field of view with ± 15° up and down. The sensor's low power consumption (∼8w), lightweight (830g), compact footprint (∼ Φ103mm*72mm), and reasonable price make it ideal for roadside deployment to serve the deer crossing detection.

The pilot site is selected at a wildlife overpass (latitude: 40.907406° N, longitude: −114.305021° E) crossing along Interstate 80 in Elko County, Nevada, United States. The historical monitoring data provided by the Nevada Department of Transportation (NDOT) shows that the frequency of wildlife using this structure to cross the road is high during migratory periods. This overpass structure was made of concrete arches and retaining walls, it is 200' long and 200' wide, and crosses over four lanes and the median. Native fill was used to backfill atop the overpass to provide a more natural pathway for movement. The exclusionary fences were built on both sides of I-80 to funnel wildlife into the entrance of the overpass. The exclusionary fence is 8' tall and consists of a woven wire mesh and support brackets. Figure 1 showed the pictures of this wildlife overpass.

This wildlife overpass is the first one over an interstate in Nevada. There is a fence deployed in the middle of the south end of the overpass, which is used to block livestock movements but will allow deer to pass. The LiDAR sensor was installed at the south end (near the middle of the fence) of

the overpass. The LiDAR sensor was mounted on a tripod for temporary data collection and powered by one deep cycle battery of the recreational vehicle (RV). The height of the LiDAR sensor should not be too high or too low since the vertical field of view only has ± 15-degree up and down range. Additionally, the location of the installation should allow the LiDAR to detect the deer on the road as far as possible. The approximate height of the LiDAR location is 5.5ft above the ground. The rotation speed of the LiDAR sensor was set as 10Hz, which allowed the sensor to obtain one data frame every 0.1 seconds. The data collection time was from 5:00 pm 3/2/2017 to 9:00 am 3/4/2017 as historical data showed that the frequency of deer using this structure was high in early March every year. A laptop was connected to the LiDAR sensor and used to process the data collected by the sensor. To evaluate the results of LiDAR data processing, a 360° camera was also set up near the sensor to help collect the movement of wildlife.

III. DEER DETECTION ALGORITHM

A new method has been developed to detect deer crossing from the LiDAR sensor. This algorithm contains three main parts: background filtering, object clustering, and object classification.

A. BACKGROUND FILTERING

The background filtering serves as the first step and basis to enhance the accuracy and computation efficiency of the subsequent data processing steps. The background filtering step needs to exclude background points (e.g., trees, ground points) but keep deer and vehicle points as much as possible. The challenge for background filtering is that the location and number of background points are not the exact same in different frames because of LiDAR vibration or dynamic moving points such as tree branches. Therefore, it is not accurate to calculate the location of background points by simply using one frame without any deer and vehicles. A background filtering method named 3D density statistic filtering (3D-DSF) was developed to exclude the background [28]. The 3D-DSF method can be elaborated into four major parts: frame aggregation, points statistics, threshold (TD) learning, and real-time filtering. Figure 2 illustrates the flowchart of background filtering.

In the frame aggregation part, the algorithm firstly overlaps multi frames collected by the LiDAR sensor into one 3D space based on their coordinates. The recommended number of frames for aggregation is between 1500 and 3000 by considering the accuracy and time cost [25]. In the points statistics step, the 3D space generated by the aggregated frames can be chopped into small cubes. The recommended side length of the cube is 0.05 cm. The practice showed that the effective detection range of VLP-16 is about 50-60 m, which is much shorter than 100 m claimed by the manufacturer. Therefore, only areas within a 60 m distance from LiDAR is considered as the region of interest (ROI). Then a 3D array is created to represent each cube in 3D space.

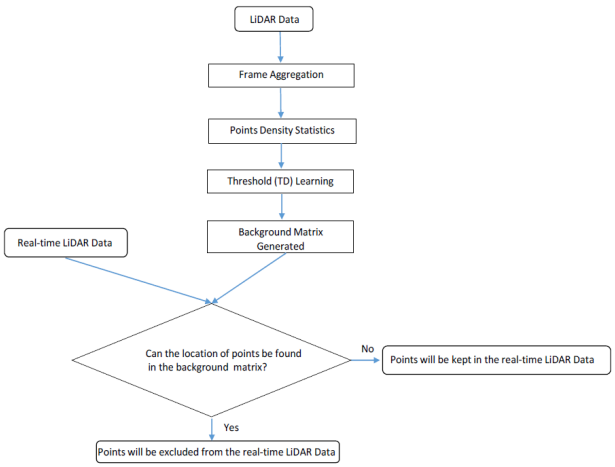

FIGURE 2. Flow chart of 3D-DSF.

The number of points in each cube can be calculated. With a pre-defined TD, each cube can be classified as background or non-background. The calculation of TD is based on the distribution of point density of the cubes in the space. There are two major factors that influence the distribution of points in the space. The first one is the distance from the object to LiDAR. In general, the number of points decreases with the increasing distance between the object and LiDAR. The whole space in the ROI is divided into several small parts based on their distance to LiDAR: 0-5 m, 5–10 m, 10–20 m, 20–30 m, 30–40 m, and longer than 40 m. So different TDs will be provided for different small parts. The second influencing factor is the existing of moving objects (deer or vehicles) in the ROI. Figure 3 shows the frequency of point density in each cube within 5 m away from LiDAR under two different scenarios after frame aggregation. It is shown that the existence of moving objects can increase the number of cubes with low point density. In other words, the deer or vehicles generate low-density cubes. If there are moving objects, the slope of the curve is smooth (Figure 3a). If no moving objects shown in the scene, the slope of the curve is uneven (Figure 3b).

Therefore, TD can be identified by Equation 1.

$$Slope = \frac{F_i - F_{i-1}}{N_i - N_{i-1}} \tag{1}$$

Ni is the ith number of points per cubic (from lowest to highest). Fi is the frequency of the ith number of points per cube. When the slope firstly becomes 0 or positive, the frequency of the number of points per cube in Equation 1 (N) is used as TD.

The background matrix can be created to represent the location of the background using the TD learned in the last step. For real-time background filtering, each frame collected by the LiDAR sensor will be transferred into a 3D matrix and compared with the matrix representing the background points. Any points found in the background matrix is then excluded from each frame.

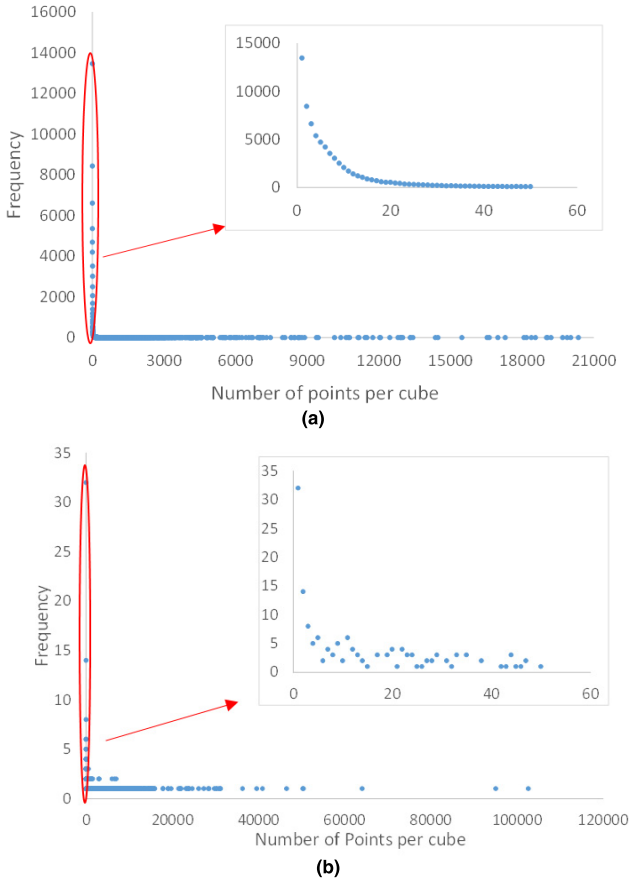

FIGURE 3. Frequency distribution of cubes with different number of points. (a) With moving objective. (b) Without moving objective.

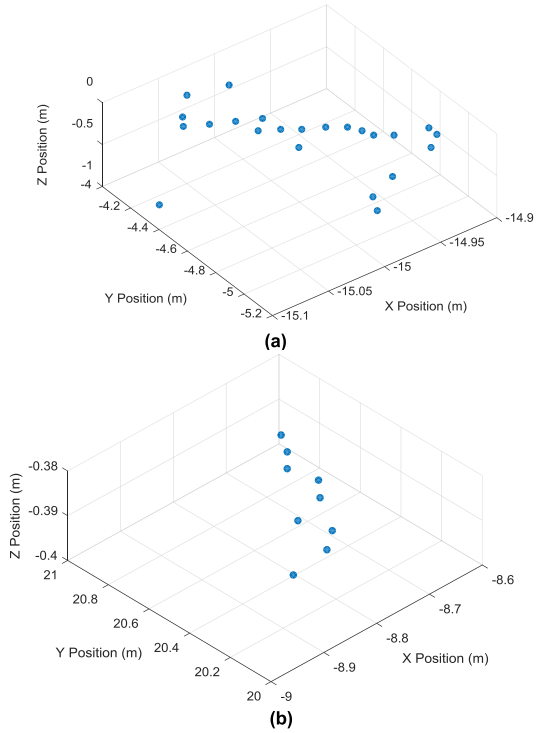

FIGURE 4. Frequency distribution of cubes with different number of points. (a) 15.548m: 23 points, (b) 21.982m: 9 points.

B. OBJECT CLUSTERING

After background filtering and lane identification, there are only deer/vehicle points left on the road. To detect the deer's location, points belonging to one deer need to be clustered into one group. Then the group can represent the deer and be continuously tracked. The previous study also showed that the point density decreases with the increasing distance to LiDAR. To give drivers enough time to react, the algorithm must detect the deer in advance, which means the deer should be identified in an extended range. There are many different algorithms available for object clustering, including k-means clustering, fuzzy clustering, and density-based clustering [29]–[31]. Density-based clustering is very suitable for vehicle clustering in LiDAR data as the point density of vehicles is much higher compared with other areas in the space. The density-based spatial clustering of applications with noise, also known as DBSCAN, is very effective to cluster density related points in the space. Another advantage of DBSCAN is this algorithm does not need to know how many vehicles are on road in one frame. DBSCAN can learn the number of clusters automatically [29]. The DBSCAN algorithm requires 2 parameters – epsilon (ε), which specifies how close points should be to each other to be considered a part of a cluster; and the minimum number of points (MinPts), which specifies how many neighbors a point should have to be included into a cluster. This paper applied DBSCAN for wildlife clustering after background filtering. Due to the angles of LiDAR laser beams and shape/size of deer and vehicles, the numbers of 3D points of deer and vehicles are different even at the same distance from the sensor. Compared to vehicles, deer are more difficult to detect with fewer points at a far distance. If an object is located near the LiDAR, intensive data points are collected and give a fine description of the object; if an object is far away from the LiDAR, only sparse data points are collected, especially for deer. Figure 4 shows the total number of 3D points of one deer located at different distances from the 16-line LiDAR.

There were only 9 points of one deer with the distance of 21.9 meters away from the LiDAR (Figure 4b), while the same deer collected 23 data points at 15.5 meters (Figure 4a), respectively.

Because of these features of roadside LiDAR data, it is difficult to obtain accurate clustering results by using a fixed MinPts value and searching radius in the traditional DBSCAN algorithm. The MinPts value and searching radius should be adjusted at different distances from the LiDAR sensor [32]. A DBSCAN-based clustering algorithm with adaptive MinPts values and ε was then developed. The selection of ε should consider the vertical angles between the laser beams of the LiDAR. This means that the searching radius should be higher than or equal to the max vertical distance between the beams to make sure the same object will not be divided into sub-objects in the vertical direction. Then the

vertical height between two adjacent points can be calculated using Equation 2.

$$H = 2d^{*}\tan(\theta/2) \tag{2}$$

where H is the vertical height between two adjacent points; d is the horizontal distance of the points to LiDAR; θ is the vertical angle of the LiDAR. The vertical angle of VLP-16 is 2°.

At a 25m distance, the vertical height between two adjacent points is H = 2d * tan (θ/2) = 2 * 25 * tan (2° /2) = 0.8725m ≈ 0.8m, so in theory, the deer (an adult deer taller than 0.8 meter) within 25m from the LiDAR can be detected successfully. However, this may be an issue when there are two deer close to each other (distance less than 0.8m). The fixed ε will cluster two deer close to each other into one large group. Therefore, the horizontal distance between two adjacent points scanned by the same laser beam is also considered. The horizontal angular resolution (α) of the VLP-16 is 0.2° with 10Hz. The horizontal distance between two adjacent points collected by the same laser can be obtained by Equation 3. This distance is the minimal searching radius in the horizontal direction for clustering point A and point B into the same cluster.

$$L = 2d^{*}\sin(\alpha/2) \tag{3}$$

where L is the horizontal distance between two adjacent points collected by the same laser (meters); d is the distance between point and LiDAR sensor (meters); α is the horizontal angular resolution of LiDAR sensor.

The adjusted method uses different radii in the vertical direction and the horizontal direction and generates an ellipsoid searching space, which can separate points of two deer close to each other. The lengths of the semi-major axis and semi-minor axis were chosen based on the vertical height H and horizontal distance L. The MinPts values were estimated based on the maximal number of points collected from the searching ellipsoid. For an ellipsoid with a semi-major axis (R_1) and a semi-minor axis (R_2), the maximal number of points (TP) that can be collected is approximately calculated by the Eqs. (4) - (6). When the laser beams shoot the ellipsoid perpendicularly, the number of points reaches maximum and the ellipsoid can be treated as an oval.

If an oval model is retained, the model has difficult to cluster the points between two ovals since the space could not be fully covered by the ovals. The oval was first approximately considered as a rectangle (size: $2R_1 * 2R_2$). The total number of lasers beams shoot on the rectangle is

$$NL = \text{floor}(\frac{2R_1}{H}) + 1 \tag{4}$$

The total number of points from each laser within the rectangle area is

$$NP = \text{floor}(\frac{2R_2}{L}) + 1 \tag{5}$$

Therefore,

$$\begin{aligned} TP &= [\text{floor}(\frac{R_1}{\text{dtan}\left(\frac{\circ}{2}\right)}) + 1]\,[\text{floor}(\frac{R_2}{\text{dsin}\left(\frac{180^{\circ} * f * n}{N_0}\right)}) + 1] \\ &\quad * \frac{\pi R_1 R_2}{2R_1 * 2R_2} \\ &= \frac{\pi}{4}[\text{floor}(\frac{R_1}{\text{dtan}\left(\frac{\circ}{2}\right)}) + 1]\,[\text{floor}(\frac{R_2}{\text{dsin}\left(\frac{180^{\circ} * f * n}{N_0}\right)}) + 1] \end{aligned} \tag{6}$$

where TP is the maximal number of points. N_0 is the total number of points per second. f is the rotation frequency of LiDAR sensor (Hz). n is the number of laser pairs. d is the distance between point and LiDAR sensor (meters). R_1 is the semi-major axis of the ellipsoid (meters). R_2 is the semi-minor axis of the ellipsoid (meters). θ is the vertical angular resolution of LiDAR sensor. Considering the angles between LiDAR laser beams and objects in real situations, the total number of points of an object is equal to or less than the calculated TP values. 40% of the TP value was selected as the MinPts value based on field data analysis.

C. OBJECT CLASSIFICATION

After object clustering, it is necessary to distinguish different types of objects. In this paper, the target of classification is to classify the object into three different groups: deer, pedestrian, and vehicle. This step can make sure vehicles and pedestrians will not be identified as deer. Appropriate features are very pivotal for object classification algorithms. For LiDAR data, the available data is point distribution (object shape). Though intensity is also reported in the point cloud, the practice shows that it is unstable and changes between different objects subject to different reflecting strength and the angles between objects to LiDAR. Therefore, this paper used features representing the shape for object classification. Inspired by the previous work [33], [34], this paper considered the following features:

- Object height in LiDAR data

It is assumed that objects move parallel along the x-y plane. The value in z-axis is the height of the object. The object height in LiDAR data may be shorter than the height of the object in the real world (consider the vertical angle of the laser beams).

- Object length in LiDAR data

All points were projected to the 2D space (x-y plane). Then the object length can be roughly calculated using Equation 7.

$$L = \max(\sqrt{(x_i^2 + y_i^2)}) \tag{7}$$

where L is the length of the object; i=1: n, n is the number of total points in the object; x is x-value of the point, y is the y-value of the point; The location of the LiDAR in the local coordinate is (0, 0).

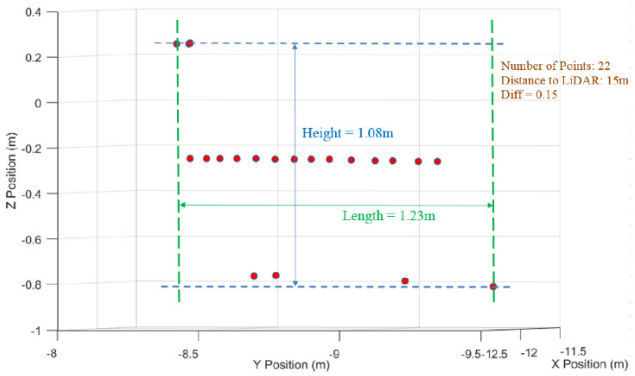

FIGURE 5. Point distribution characteristics of one deer.

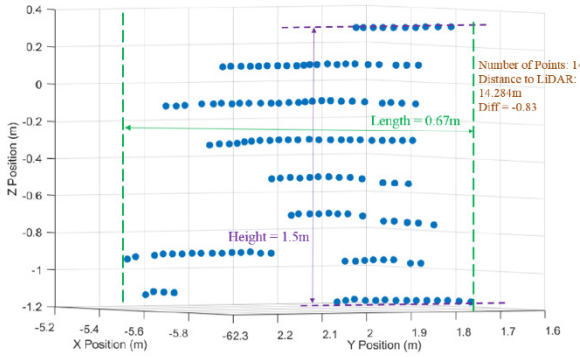

FIGURE 6. Point distribution characteristics of one pedestrian.

- Nearest distance from object points to LiDAR

The nearest distance can be calculated using Equation 8.

$$\mathrm{D} = \min(\sqrt{(x_i^2 + y_i^2 + z_i^2)}) \tag{8}$$

where D is the nearest distance from the points group to LiDAR; i = 1: n, n is the number of total points in the object; x is x-value of the point, y is the y-value of the point, z is the z-value of the point; The location of the LiDAR in the local coordinate is (0, 0, 0).

- Number of points
- Primary direction of points distribution

We compare the length and height of the objects. It can be found that for deer and vehicles, the length is larger than the height, while for pedestrian, the height is larger than the length (for adult only). Therefore, we use Equation 9 to represent the direction of points distance. This feature can be very helpful to distinguish deer and pedestrians.

$$\mathrm{Diff} = \mathrm{L} - \mathrm{D} \tag{9}$$

where Diff is the difference between length and height; L is the length of the object; D is the height of the object. If Diff > 0, it means the primary direction is along the x-y plane and if Diff < 0, it means the primary direction is along z-axis.

Figure 5∼Figure 7 showed that the point distribution characteristics of deer, vehicle and pedestrian are different from each other. Figure 5 showed an example of the feature selection of one deer. The height of the deer in the LiDAR is 1.08m. The length of the deer is 1.23m. The number of points in this cluster is 22. Diff of the deer is 0.15 ($1.23 - 1.08 = 0.15$). The primary direction is along the x-y plane.

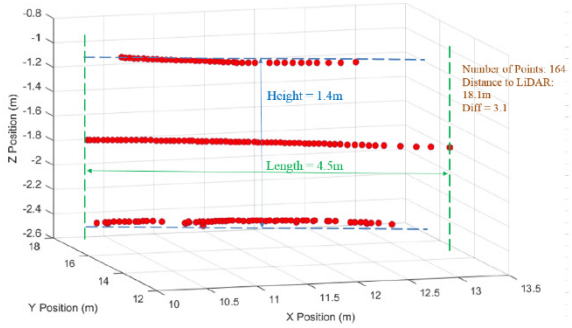

FIGURE 7. Point distribution characteristics of one vehicle.

Figure 6 showed an example of the feature selection of one pedestrian. The height of the pedestrian in the LiDAR is 1.5m. The length of the pedestrian is 0.67m. The number of points in this cluster is 145. Diff of the pedestrian is -0.83 ($0.67 - 1.5 = -0.83$). The primary direction is along z-axis.

Figure 7 showed an example of the feature selection of one vehicle. The height of the vehicle in the LiDAR is 1.4m. The length of the vehicle is 4.5m. The number of points in this cluster is 164. Diff of the vehicle is 3.1 ($4.5 - 1.4 = 3.1$). The primary direction is along the x-y plane.

It should be noted that the deer and vehicle/pedestrian data were collected separately as it was not easy to capture the event that deer were crossing the road while vehicles were on the road. The vehicle data were collected by the LiDAR sensor deployed near the wildlife overpass on the I-80 freeway and the pedestrian data were collected by the LiDAR sensor deployed at several urban intersections in Reno, Nevada. A total of 157 pedestrian records, 419 vehicle records (including 202 passenger cars, 103 bus, and 114 different types of trucks) were generated and manually marked. For the deer records, only 8 deer were collected. To expand the sample size of the deer, we extracted the information of the deer at various locations (for the same deer, the detected length, height, number of points et al. changed at different frames). Therefore, a total of 1,359 deer records were generated (from the trajectories of eight deer).

A lot of algorithms have been developed for object clustering, including naive Bayes classifier (NB) [35], random forest classifiers (RF) [36], K-nearest neighbor classification (KNN) [37], Support Vector Machine (SVM) [38], and neural network [39]. Each method has its own strengths and weaknesses regarding accuracy, performance, and ease of use. In this paper, we compared the performance of RF, NB, and KNN considering the ease of use. The brief description of the three methods was introduced as follows:

- RF is an ensemble of multiple trees. The RF works better than single decision tree because a single decision tree may be prone to a noise, but the aggregate of many decision trees can reduce the effect of noise and give

TABLE 1. Confusion matrix.

RF					
			Actual Class		
			Deer	Pedestrian	Vehicle
Training Database	Predicted Class	Deer	952	1	1
		Pedestrian	0	108	1
		Vehicle	0	1	292
			Actual Class		
			Deer	Pedestrian	Vehicle
Testing Database	Predicted Class	Deer	407	0	0
		Pedestrian	0	47	1
		Vehicle	0	0	124
NB					
			Actual Class		
			Deer	Pedestrian	Vehicle
Training Database	Predicted Class	Deer	949	0	3
		Pedestrian	0	108	1
		Vehicle	3	2	292
			Actual Class		
			Deer	Pedestrian	Vehicle
Testing Database	Predicted Class	Deer	406	0	0
		Pedestrian	0	47	1
		Vehicle	1	0	124
KNN					
			Actual Class		
			Deer	Pedestrian	Vehicle
Training Database	Predicted Class	Deer	952	1	1
		Pedestrian	0	105	2
		Vehicle	0	4	291
			Actual Class		
			Deer	Pedestrian	Vehicle
Testing Database	Predicted Class	Deer	407	1	0
		Pedestrian	0	42	1
		Vehicle	0	4	124

more accurate results. The training algorithm for random forests applies the general technique of bootstrap aggregating, or bagging, to tree learners. After training, predictions for unseen samples x' can be made by averaging the predictions from all the individual regression trees on x' [40], [41].

- NB is based on the assumption that each feature is statistically independent, the probability density function (pdf) that characterizes the object class is modeled as the product of each feature-based pdf [42], [43].
- KNN is an instance-based classification method. An object is classified by a majority vote of its neighbors, with the object being assigned to the class most common among its k nearest neighbors [44].

The confusion matrix of the three methods is documented in Table 1.

The results show most objects are classified to their corresponding group correctly, except for few mis-classified ones. The confusion matrix showed that the most common mis-classified type was pedestrian ↔ vehicle (wrong classification between vehicle and pedestrian). By manually checking the data, it was found that the features of a few pedestrians were significantly different from the others when the pedestrian was carrying big items or the pedestrians was running. Under those situations, the primary direction of point distribution and/or the object length were different from those of the normal walking pedestrians.

TABLE 2. Performance comparison of RF, NB, and KNN.

	RF		NB		KNN	
Dataset	TR	TE	TR	TE	TR	TE
Total Clusters	1,356	579	1,356	579	1,356	579
Deer	952	407	952	407	952	407
Pedestrians	110	47	110	47	110	47
Vehicles	294	125	294	125	294	125
Identified Deer	954	407	952	406	954	408
Identified Pedestrians	109	48	109	48	107	43
Identified Vehicles	293	124	295	125	295	128
Accuracy	99.7%	99.8%	99.3%	99.6%	99.4%	98.9%

TR is "training set " and TE is "testing set"

Table 2 summarizes the performance of different algorithms. It is shown that all the three algorithms can provide high accuracy (more than 98%) of object classification. RF has a slightly higher accuracy (99.8%) compared to the other two methods. Therefore, RF is recommended to be used for object clustering in this paper.

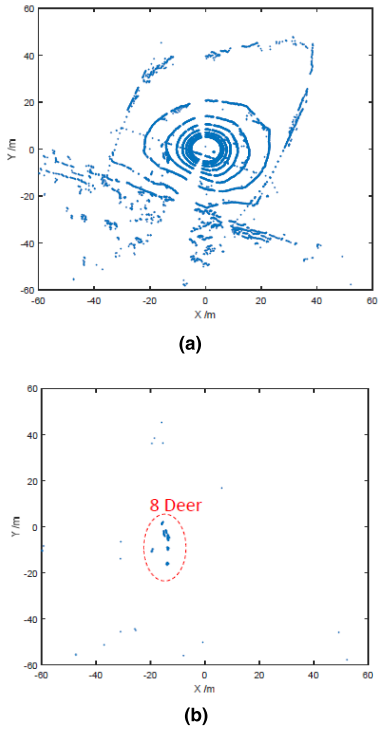

FIGURE 8. Before-after background filtering. (a) Before background filtering. (b) After background filtering.

IV. RESULTS OF DEER CROSSING DETECTION

The results of data processing showed that eight deer crossed the road using the overpass in the morning of 3/3/2017, from 6:45:36 am to 6:47:46 am. These deer moved in a group and were all detected by the LiDAR. Since the deer crossing occurred in the early morning, the 360° camera did not provide a clear record for this movement limited to the insufficient light condition.

After obtaining the location of the background points, the 3D-DSF only needs about 100 ms to exclude the background, which can serve the real-time data processing task. Figure 8 demonstrates one frame before and after background filtering collected at the wildlife overpass.

In this frame, there were 13,561 points in the raw data (Figure 8a). After background filtering (Figure 8b), only 30 points were left in the space, which meant that 99% of background points were successfully excluded. At the same time, more than 94% of deer points were kept after background filtering. Table 3 shows the details of the before-and-after statistical results. The statistical results showed that the 3D-DSF can exclude the background points effectively.

After object clustering and classification, the deer can be detected. Figure 9 showed the example of deer detection. It is difficult to tell how many deer in the raw data (Figure 9a), with the developed algorithm, eight deer were identified by the LiDAR sensor (Figure 9b).

In this example, all objects were detected as deer by RF correctly. As mentioned before, in some frames, only six or seven deer were detected as some deer appear to have been

TABLE 3. Performance of 3D-DSF.

	Before 3D-DSF	After 3D-DSF
Total Number of Points	13,561	370
Background Points	13,210	30
Background Filtering Percentage	30/13,210*100%=99.8%	
Deer Points	351	330
Deer excluded percentage	(351-330)/351*100%=5.98%	

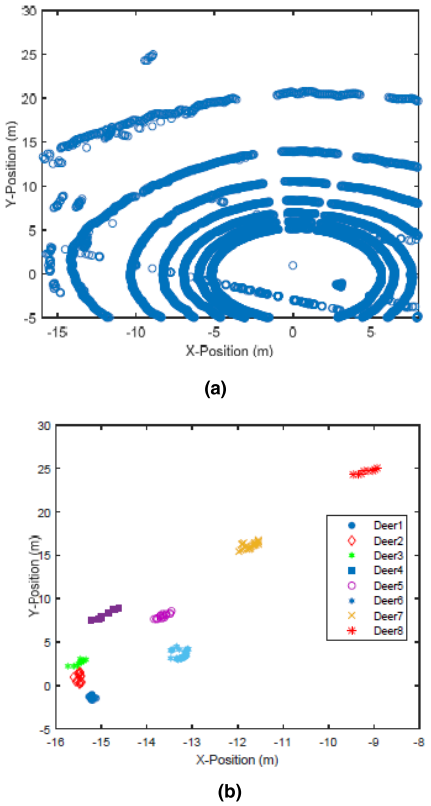

FIGURE 9. Captured deer crossing activity. (a) Raw LiDAR data. (b) Clustered results.

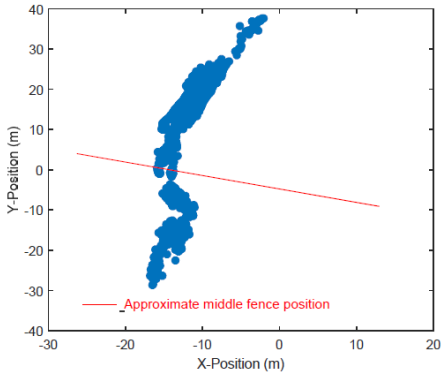

FIGURE 10. Trajectories of deer.

blocked by the other deer or the middle fence, which may not be successfully captured by LiDAR sensor. After collecting all the points of deer, the trajectories of the deer group can be generated, as illustrated in Figure 10.

TABLE 4. Detection range.

	#1	#2	#3	#4	#5	#6	#7	#8
Max Detection Distance (m)	31.8	37.7	32.8	29.6	27.7	27.5	32.3	26.3
Average Detection Range of Deer (m)	30.7							

It is shown that deer moved from the west to the east direction in a group. The video uploaded to YouTube (https://www.youtube.com/watch?v = qnvdSN6iusI&feature =youtu.be) showed that_deer changed their moving direction a little bit when approaching the middle fence. While deer were gathered near the fence preparing to jump, some deer were blocked by the others or the middle fence. As a result, the beam of the LiDAR sensor could not detect all deer in some frames. Therefore, there are some data gaps near the fence. Table 4 shows the distance of the deer to LiDAR when it is first detected.

The detection range varies in relation to different distances and angles from the LiDAR. The average detection range was 30.72 m from the LiDAR sensor. The max effective detection range obtained by the algorithm was 37.74 m. While deer can be seen in the LiDAR video outside of the 37.74m max detection range, the algorithm was unable to identify those points as deer. The detection range can be extended by deploying and integrating multiple LiDAR sensors in the detection area. In theory, once one deer is detected, the light on the sign can be trigged to flash to warn the drivers. This can give drivers enough time to slow down.

The algorithm has been implemented in Matlab and was deployed on a Dell desktop equipped with an Intel Core i7-4790 CPU (3.60GHz) and 16 GB of RAM. After obtaining the location of the background-3D matrix, the time used to identify deer from one frame is about 200ms, which can meet the requirement of real-time data processing.

V. DISCUSSION

There is still a lot of room for improvement for deer detection. This paper did not provide a reliable algorithm for deer tracking. For safety application, it may not be necessary to track the same deer. If one deer is detected by the LiDAR, the warning system can be activated. When all deer were out of the detection range of the LiDAR, the warning system can be turned off. But for wildlife biology research, it is interesting to see the detailed movement (speed and location) of the deer. The blocked deer and deer close to each other increased the challenge to track the individual deer in a spare point cloud. The authors applied the Global Nearest Neighbor (GNN) [45] to track the same vehicles in different frames in a previous study [25]. The practice using GNN for tracking deer showed that if the speed of the deer was high and there was another deer close to it, then the label might be assigned to another deer incorrectly. If the deer was completely blocked in one frame, then the label of the deer was discarded. Considering the challenge in tracking the blocked deer and deer group, the speed calculation of the deer is not accurate. The GNN algorithm could not provide reliable speed and location for these deer blocked by the others. Therefore, this paper did not analyze the trajectory of the individual deer. Multi-LiDAR installed in different directions can be an option to improve the accuracy. If multi-LiDARs are installed in different directions, even the deer is not visible in one LiDAR, it may be visible in other LiDARs. Since the multi-LiDARs can increase the number of points for the objects, the shape of the deer in LiDAR data can be clearer [46].

In this pilot field test, the sensor was powered by the battery which needs to be charged every day. In the future, it is recommended to charge the battery using solar energy which will dramatically reduce maintenance costs. The wildlife detection algorithm in this paper provided the method to distinguish between wildlife and vehicles. Additionally, the speed can be used to distinguish deer and vehicles as the speed limit on roads is higher compared to the speed of typical deer movements. A more detailed study with a longer data collection period is expected to be conducted to capture wildlife crossing the road, which can be used to evaluate the effectiveness of the wildlife and vehicle division method.

To further improve the accuracy of object classification, the lane identification may be used to distinguish deer group and a vehicle. The lane identification can generate the boundaries of the road. With the assumption that vehicles moving on the road and deer moving off the road, the deer group may be distinguished from a vehicle. Subject to the limited data, this paper did not implement this into the procedure. For small animals like a hare or squirrel, the LiDAR may not scan enough points for clustering. Therefore, the LiDAR roadside is only effective to detect larger animals such as deer or horse detection. The main purpose of this research is to serve traffic safety. So small animals should not be a problem for traffic safety. Considering the limitation of the current algorithms and the challenge in deer tracking using roadside LiDAR, it is suggested to use LiDAR as auxiliary equipment, working together with cameras for wildlife detection.

VI. CONCLUSIONS

This paper provides a new and cost-effective approach to detecting deer crossing road with 360° LiDAR sensors. The procedure developed in this paper includes background filtering, object clustering, and object classification. The field test shows that the algorithm can detect deer with a max radius of 37.74m (124ft) around the LiDAR sensor. This real-time information can be used to trigger flashing warning signs to provide warning information to drivers. This innovative data collection approach can also be used to analyze wildlife behavior. Considering the different crossing structures built along I-80, this method can also be deployed along different crossing structures to evaluate the effects of the different

structures with the understanding of wildlife-crossing patterns [46]. It should be mentioned that the object occlusion issue can greatly influence the accuracy of deer detection and tracking. An easy and effective solution is to install another LiDAR in different directions. However, different LiDARs generate the point cloud in their own local coordinate system. How to integrate point cloud from different LiDAR sensors is another topic for future studies [47]. The wildlife information and vehicle trajectories could even be integrated and broadcasted through the connected vehicle communication system to support future autonomous and connected vehicles. It is best suited for targeted areas rather than being deployed at regular intervals along a large stretch of road considering the current high cost of LiDAR sensors. For instance, this technology would be useful at the ends of fencing. This research can be considered as a first step to develop the real-time deer crossing warning system.

More field test is expected to be conducted to further evaluate the proposed algorithm. The LiDAR sensor does not work well in some environments such as rain, snow, fog, and dust. This research did not test the performance of the algorithm under bad weather situations limited to the unavailable data. This paper did not test the minimum size of the deer that can be detected by our algorithm also due to the unavailable data. This research combined the basic models for the real-time deer crossing detection. The tradeoff here is that the advanced models usual have high computational load to achieve the high accuracy. Our proposed method has low computational load and can achieve a relatively high accuracy (though could not reach the global best). Testing the performance of other advanced detection models will be investigated in the next step.

REFERENCES

[1] J. H. Hedlund, P. D. Curtis, G. Curtis, and A. F. Williams, "Methods to reduce traffic crashes involving deer: What works and what does not," *Traffic Injury Prevention*, vol. 5, no. 2, pp. 122–131, 2004.

[2] A. Clevenger and M. P. Huijser, "Wildlife crossing structure handbook, design and evaluation in north america," Dept. Transp., Federal Highway Admin., Washington, DC, USA, Tech. Rep. FHWA-CFL/TD-11-003, 2011.

[3] M. P. Huijser, J. A. Fuller, M. E. Wagner, A. Hardy, and A. Clevenger, "Animal–vehicle collision data collection. A synthesis of highway practice," Nat. Cooperat. Highway Res. Program Synth., Transp. Res. Board, Washington, DC, USA, Tech. Rep. SYNTHESIS 370, 2007.

[4] F. Viani, F. Robol, E. Giarola, G. Benedetti, S. De Vigili, and A. Massa, "Advances in wildlife road-crossing early-alert system: New architecture and experimental validation," in *Proc. 8th Eur. Conf. Antennas Propag.*, Apr. 2014, pp. 3457–3461.

[5] T. M. Pojar, R. A. Prosence, D. F. Reed, and T. N. Woodard, "Effectiveness of a lighted, animated deer crossing sign," *J. Wildlife Manage.*, vol. 39, no. 1, pp. 87–91, Jan. 1975.

[6] J. M. Krisp and S. Durot, "Segmentation of lines based on point densities—An optimisation of wildlife warning sign placement in southern Finland," *Accident Anal. Prevention*, vol. 39, no. 1, pp. 38–46, Jan. 2007.

[7] S. Piry, A. Alapetite, J.-M. Cornuet, D. Paetkau, L. Baudouin, and A. Estoup, "GENECLASS2: A software for genetic assignment and first-generation migrant detection," *J. Heredity*, vol. 95, no. 6, pp. 536–539, Nov./Dec. 2004.

[8] P. Juang, H. Oki, Y. Wang, M. Martonosi, L. S. Peh, and D. Rubenstein, "Energy-efficient computing for wildlife tracking: Design tradeoffs and early experiences with ZebraNet," *ACM SIGARCH Comput. Archit. News*, vol. 30, no. 5, pp. 96–107, 2002.

[9] F. Urbano, F. Cagnacci, C. Calenge, H. Dettki, A. Cameron, and M. Neteler, "Wildlife tracking data management: A new vision," *Philos. Trans. Roy. Soc. B, Biol. Sci.*, vol. 365, no. 1550, pp. 2177–2185, 2010.

[10] A. T. Ford, A. P. Clevenger, and A. Bennett, "Comparison of methods of monitoring wildlife crossing-structures on highways," *J. Wildlife Manage.*, vol. 73, no. 7, pp. 1213–1222, 2009.

[11] J. Wu, "Effect and influence of different factors on driver behavior when vehicles make right turns at signalized intersections," *SHRP 2 Saf. Data Student Paper Competition*, vol. 221, pp. 24–32, May 2017.

[12] M. Steinbach, G. Karypis, and V. Kumar, "A comparison of document clustering techniques," in *Proc. KDD Workshop Text Mining*, 2000, vol. 400, no. 1, pp. 525–526.

[13] H. Sandhawalia, J. A. Rodriguez-Serrano, H. Poirier, and G. Csurka, "Vehicle type classification from laser scanner profiles: A benchmark of feature descriptors," in *Proc. 16th Int. IEEE Conf. Intell. Transp. Syst.*, Oct. 2013, pp. 517–522.

[14] P. Christiansen, K. A. Steen, R. N. Jørgensen, and H. Karstoft, "Automated detection and recognition of wildlife using thermal cameras," *Sensors*, vol. 14, no. 8, pp. 13778–13793, 2014.

[15] R. Gade and T. B. Moeslund, "Thermal cameras and applications: A survey," *Mach. Vis. Appl.*, vol. 25, no. 1, pp. 245–262, 2014.

[16] F. Viani, P. Rocca, L. Lizzi, M. Rocca, G. Benedetti, and A. Massa, "WSN-based early alert system for preventing wildlife-vehicle collisions in Alps regions," in *Proc. IEEE-APS Top. Conf. Antennas Propag. Wireless Commun.*, Sep. 2011, pp. 106–109.

[17] W. Butler, "Design considerations for intrusion detection wide area surveillance radars for perimeters and borders," in *Proc. IEEE Conf. Technol. Homeland Secur.*, May 2008, pp. 47–50.

[18] K. A. Steen, A. Villa-Henriksen, O. R. Therkildsen, and O. Green, "Automatic detection of animals in mowing operations using thermal cameras," *Sensors*, vol. 12, no. 6, pp. 7587–7597, 2012.

[19] J. Wu, H. Xu, Y. Sun, J. Zheng, and R. Yue, "Automatic background filtering method for roadside LiDAR data," *Transp. Res. Rec.*, vol. 2672, no. 45, pp. 106–114, 2018.

[20] J. Wu, H. Xu, and J. Zheng, "Automatic background filtering and lane identification with roadside LiDAR data," in *Proc. 20th Int. Conf. Intell. Transp. Syst.*, Oct. 2017, pp. 1–6.

[21] S. A. Gargoum, K. El-Basyouny, and J. Sabbagh, "Assessing stopping and passing sight distance on highways using mobile LiDAR data," *J. Comput. Civil Eng.*, vol. 32, no. 4, 2018, Art. no. 04018025.

[22] C. Ai and Y.-C. J. Tsai, "Critical assessment of an enhanced traffic sign detection method using mobile LiDAR and INS technologies," *J. Transp. Eng.*, vol. 141, no. 5, May 2015, Art. no. 04014096.

[23] A. Shams *et al.*, "Highway cross-slope measurement using mobile LiDAR," *Transp. Res. Rec.*, vol. 2672, no. 39, pp. 88–97, 2018.

[24] C. Ai and Y. Tsai, "Automated sidewalk assessment method for americans with disabilities act compliance using three-dimensional mobile LiDAR," *Transp. Res. Rec.*, vol. 2542, no. 1, pp. 25–32, 2016.

[25] H. Xu and J. Wu, "An automatic procedure for vehicle tracking with a roadside LiDAR sensor," in *Proc. 97th Annu. Transp. Res. Board Meeting*, Washington, DC, USA, 2018.

[26] J. Wu, H. Xu, and J. Zhao, "Automatic lane identification using the roadside LiDAR sensors," *IEEE Intell. Transp. Syst. Mag.*, to be published.

[27] Y. Zheng, H. Xu, Z. Tian, and J. Wu, "Design and implementation of the DSRC-Bluetooth communication and mobile application with LiDAR sensor," in *Proc. 97th Annu. Transp. Res. Board Meeting*, Washington, DC, USA, 2018.

[28] J. Wu, H. Xu, Y. Zheng, and Z. Tian, "A novel method of vehicle-pedestrian near-crash identification with roadside LiDAR data," *Accident Anal. Prevention*, vol. 121, pp. 238–249, Dec. 2018.

[29] M. Ester, H.-P. Kriegel, J. Sander, and X. Xu, "A density-based algorithm for discovering clusters in large spatial databases with noise," in *Proc. KDD*, Aug. 1996, vol. 96, no. 34, pp. 226–231.

[30] N. R. Pal, K. Pal, J. M. Keller, and J. C. Bezdek, "A possibilistic fuzzy c-means clustering algorithm," *IEEE Trans. Fuzzy Syst.*, vol. 13, no. 4, pp. 517–530, Aug. 2005.

[31] T. Kanungo, D. M. Mount, N. S. Netanyahu, C. D. Piatko, R. Silverman, and A. Y. Wu, "An efficient K-means clustering algorithm: Analysis and implementation," *IEEE Trans. Pattern Anal. Mach. Intell.*, vol. 24, no. 7, pp. 881–892, Jul. 2002.

[32] H. Zhou, P. Wang, and H. Li, "Research on adaptive parameters determination in DBSCAN algorithm," *J. Inf. Comput. Sci.*, vol. 9, no. 7, pp. 1967–1973, 2012.

[33] J. Zhao, H. Xu, D. Wu, and H. Liu, "An artificial neural network to identify pedestrians and vehicles from roadside 360-degree LiDAR data," in *Proc. 97th Annu. Transp. Res. Board Meeting*, Washington, DC, USA, 2018.
[34] H. Lee and B. Coifman, "Side-fire lidar-based vehicle classification," *Transp. Res. Rec.*, vol. 2308, no. 1, pp. 173–183, 2012.
[35] K. P. Murphy, *Naive Bayes Classifiers*. Vancouver, BC, Canada: Univ. British Columbia, 2006.
[36] L. Breiman, "Random forests," *Mach. Learn.*, vol. 45, no. 1, pp. 5–32, Oct. 2001.
[37] D. Li, K. D. Wong, Y. H. Hu, and A. M. Sayeed, "Detection, classification, and tracking of targets," *IEEE Signal Process. Mag.*, vol. 19, no. 2, pp. 17–29, Mar. 2009.
[38] Z. Sun and X. Ban, "Vehicle classification using GPS data," *Transp. Res. C, Emerg. Technol.*, vol. 37, pp. 102–117, Dec. 2013.
[39] G. Zhang, Y. H. Wang, and H. Wei, "Artificial neural network method for length-based vehicle classification using single-loop outputs," *Transp. Res. Rec.*, vol. 1945, no. 1, pp. 100–108, 2006.
[40] A. González, D. Vázquez, A. M. López, and J. Amores, "On-board object detection: Multicue, multimodal, and multiview random forest of local experts," *IEEE Trans. Cybern.*, vol. 47, no. 11, pp. 3980–3990, Nov. 2017.
[41] M. Khalilikhah, G. Fu, K. Heaslip, and P. Carlson, "Analysis of in-service traffic sign visual condition: Tree-based model for mobile LiDAR and digital photolog data," *J. Transp. Eng., A, Syst.*, vol. 144, no. 6, 2018, Art. no. 04018017.
[42] C. Premebida, O. Ludwig, and U. Nunes, "LIDAR and vision-based pedestrian detection system," *J. Field Robot.*, vol. 26, no. 9, pp. 696–711, Sep. 2009.
[43] N. S. Altman, "An introduction to kernel and nearest-neighbor nonparametric regression," *Amer. Statistician*, vol. 46, no. 3, pp. 175–185, 1992.
[44] M. Tan, B. Wang, Z. Wu, J. Wang, and G. Pan, "Weakly supervised metric learning for traffic sign recognition in a LIDAR-equipped vehicle," *IEEE Trans. Intell. Transp. Syst.*, vol. 17, no. 5, pp. 1415–1427, May 2016.
[45] P. Konstantinova, A. Udvarev, and T. Semerdjiev, "A study of a target tracking algorithm using global nearest neighbor approach," in *Proc. Int. Conf. Comput. Syst. Technol.*, 2003, pp. 290–295.
[46] J. Wu, "Data processing algorithms and applications of LiDAR-enhanced connected infrastructure sensing," Ph.D. dissertation, Univ. Nevada Reno, Reno, NV, USA, 2018.
[47] J. Wu, H. Xu, and W. Liu, "Points registration for roadside LiDAR sensors," *Transp. Res. Rec. J. Transp. Res. Board*, to be published. doi: 10.1177/0361198119843855.

JINGRONG CHEN received the B.S. degree from the Department of Mathematics, Beijing Jiaotong University, Beijing, China, in 1997, the M.S. degree from the School of Mathematics, Lanzhou University, Lanzhou, China, in 2004, and the Ph.D. degree from the School of Traffic and Transportation, Lanzhou Jiaotong University, Lanzhou, in 2009. Her current research interests include intelligent transportation systems, network optimization, and multi-objective decision-making.

HAO XU received the bachelor's and master's degrees from the Department of Automation, University of Science and Technology of China, in 2004 and 2007, respectively, and the master's and Ph.D. degrees in civil engineering from the Texas Tech University, in 2009 and 2010, respectively. From 2010 to 2013, he was a Postdoctoral Research Associate with the Texas Tech University. Since 2013, he has been an Assistant Professor with the Department of Civil and Environmental Engineering, University of Nevada, Reno. His current research interests include connected-vehicle applications with roadside LiDAR sensors, driving behavior analysis, traffic safety, and fuel consumption evaluation. He manages the connected-vehicle testing environment at the University of Nevada. The testing environment promotes interdisciplinary research on connected/autonomous vehicles to improve traffic safety and mobility. His research team has set up a LiDAR-based connected intersection in Reno, and is performing research on LiDAR-based connected infrastructures.

JIANQING WU received the B.S. and M.S. degrees in civil engineering from Shandong University, Jinan, China, in 2012 and 2015, respectively, and the Ph.D. degree from the Department of Civil and Environmental Engineering, University of Nevada, Reno, in 2018, where he is currently a Postdoctoral Research Associate. His current research interests include driver behavior analysis, intelligent transportation systems, traffic safety, and big data processing.

RUI YUE received the B.S. degree from the Beijing Jiaotong University, in 2015, and the M.S. degree from the University of Nevada, Reno, in 2017, where he is currently pursuing the Ph.D. degree with the Department of Civil and Environment. His research interests include traffic signal control, traffic operations, and GIS application in Transportation.

CHANGWEI YUAN received the M.S. and Ph.D. degrees from the School of Economics and Management, Chang'an University. He had been a Postdoctoral Research Associate with Tsinghua University before his faculty career at Chang'an University. He is currently a Professor with the School of Economics and Management, Chang'an University. His research interests include traffic planning and operation, industrial economics, and intelligent transportation systems.

LU WANG received the B.S. and M.S. degrees in civil engineering from Shandong University, Jinan, China, in 2014 and 2017, respectively. She is currently pursuing the Ph.D degree with the Department of Civil and Environmental Engineering, University of Nevada, Reno, NV, USA. Her research interests include intelligent transportation systems and traffic safety.